

Structure/Function Assessment of Synapses at Motor Nerve Terminals

A.F.M. JOHNSTONE,¹ K. VIELE,² AND R.L. COOPER^{1*}

¹Department of Biology, University of Kentucky, Lexington, Kentucky 40506-0225

²Department of Statistics, University of Kentucky, Lexington, Kentucky 40506-0027

KEY WORDS Active zone, quantal, neuromuscular junction, reconstruction, electron microscopy

ABSTRACT The release of transmitter at neuromuscular junctions (NMJ) of the opener muscle in crayfish is quantal in nature. This NMJ offers the advantage of being able to record quantal events at specific visually identified release sites, thus allowing measurement of the physiological parameters of vesicle release and its response to be directly correlated with synaptic structure. These experiments take advantage of areas between the varicosities on the nerve terminal that we define as “stems.” Stems were chosen as the region to study because of their low synaptic output due to fewer synaptic sites. Through 3D reconstruction from hundreds of serial sections, obtained by transmission electron microscopy (TEM), at a site in which focal macropatch recordings were obtained, the number of synapses and AZs are revealed. Thus, physiological profiles with various stimulation conditions can be assessed in regards to direct synaptic structure. Here, we used the properties of the quantal shape to determine if distinct subsets of quantal signatures existed and if differences in the distributions are present depending on the frequency of stimulation. Such a quantal signature could come about by parameters of area, rise time, peak amplitude, latency, and tau decay. In this study, it is shown that even at defined sites on the stem, with few active zones, synaptic transmission is still complex and the quantal responses appear to be variable even for a given synapse over time. In this study, we could not identify a quantal signature for the conditions utilized. **Synapse 65:287–299, 2011.** © 2010 Wiley-Liss, Inc.

INTRODUCTION

Evoked neurotransmitter release is dependent on depolarization induced calcium ion (Ca^{2+}) influx through specific voltage gated channels on the pre-synaptic terminal (Augustine et al., 1985; Augustine 2001; Llinas et al., 1981; Sugimori et al., 1994; Zucker et al., 1991). This Ca^{2+} influx induces vesicle fusion through protein interactions (i.e., syntaxin, synaptobrevin, synaptotagmin and numerous others; Sudhof, 1995, 2004). This influx is essential for transmitter release (Katz and Miledi, 1967, 1968). Freeze-fracture and transmission electron micrographs (TEM) reveal groups of intramembraneous entities. These structures are assumed to be Ca^{2+} and other ion channel proteins that are in close association with sites of vesicular fusion (Cooper et al., 1996b; Couteaux and Pecot-Dechavassine, 1970; Govind et al., 1994; Heuser and Reese, 1974). In many cases there appears to be a dense structure, which exists in a broad variety of shapes from species to species, in close apposition where vesicles fuse to the inner face of the presynap-

tic membrane. For example, the salamander retinal rod synapse shows an array of dense bars lined with ribbons of synaptic vesicles aligned for docking (Rao-Mirotnik et al., 1995). At the frog neuromuscular junction (NMJ) there are long dense bars in which vesicles associate (Kriebel et al., 2000). At the crayfish excitatory neuromuscular junction, a dense body in the shape of a hemisphere is present with vesicles docked in a circular array around the dense mound (Jahromi and Atwood, 1974). The dense structures in synapses in the CNS of mammals align themselves in

Contract grant sponsor: NSF; Contract grant number: NSF-IBN-0131459; Contract grant sponsor: NIH; Contract grant number: NCRR P20RR16481; Contract grant sponsor: School of Biological Sciences at the University of Kentucky; G. Ribble Fellowship for graduate studies in the Dept of Biology, University of Kentucky for A.F.M.J.

*Correspondence to: Robin L. Cooper, 675 Rose Street, Dept. of Biology, University of Kentucky, Lexington, KY 40506-0225, USA.
E-mail: RLCOOP1@pop.uky.edu

Received 8 March 2010; Accepted 21 July 2010

DOI 10.1002/syn.20847

Published online 20 August 2010 in Wiley Online Library (wileyonlinelibrary.com).

an organized array on the synapse that works as an entire unit (Vrensen, 1980). Although the dense body is not completely understood nor its makeup revealed, it is a constant indicator from species to species as the site of vesicular accumulation. The colocalization of these structures, the dense body and intramembraneous particles are indicative of the synaptic active zone (AZ) on the presynaptic terminal (Couteaux, 1970; Couteaux and Pecot-Dechavessine, 1974).

Evidence supports that the structural makeup of the synapse, in relation to AZs in multiple vertebrate and invertebrate models, is a component that is correlated with the amount of evoked transmitter release (Cooper et al., 1996a,b; Rheuben, 1985; Walrond and Reese, 1985). One advantage of the invertebrate crustacean model for synaptic transmission is that physiological recordings can be directly associated with synaptic ultrastructure. The structural components may be identified with TEM. The number and size of synapses, number of active zones, and abundance of vesicular pools (i.e., docked vesicles or those in readily release or reserve pools) are the structures readily able to be quantified. Another advantage of the crustacean NMJ is that the precise area that was physiologically assessed can be rebuilt in 3D. The crayfish opener muscle is a preparation that allows many of the problems associated with quantal currents and the analysis to be kept at a minimum (Cooper et al., 1995b). Thus, insight into whether ultrastructure correlates to the physiological recorded quantal events is ascertainable (Cooper et al., 1995a, 1996a). Although it was previously shown how the spacing of active zones and their relative distances to calcium channels can affect the probability that a vesicle will fuse with the presynaptic membrane (Cooper et al., 1996b), it does not account for the quantal current variability seen when recording from synaptic sites. Because of this variability, one could assume that there are multiple sites that may be active within a recorded location. In a past study of these terminals, single-evoked responses were examined and characterized at low-frequency stimulation (Lancaster et al., 2007). The results indicated that there groupings in the characteristics in the quantal recordings such as size, shape, rise times, and decay constants. This hinted at the possibility of identifying a "quantal signature" for a given synapse.

Del Castillo and Katz (1954a,b) showed transmitter released from the frog NMJ is quantal in nature, which is also true for the crayfish NMJ (Cooper et al., 1995a; Dudel, 1981). The concept of this quantal nature has been confirmed for many different synapses from multiple species, including mammalian CNS neurons (Hessler et al., 1993; Redman, 1990; Rosemund et al., 1993). Characterization of transmission and alterations demands measurement at the quantal content level for understanding the pre- and postsynaptic mechanisms involved. Assessing these charac-

teristics is better approached in some systems. Here we used a macro-patch technique to investigate identified sites of synaptic transmission and various stochastic methods to examine quantal groupings of individual synaptic currents. One approach was to cluster the various quantal characteristics and determine if there are populations of quantal units. Initially the peak amplitude and the area of depolarization wave form were used to examine for quantal clustering using Gaussian Mixture models (Viele et al., 2003). With this approach the change in the quantal occurrence within a defined population or if a new population appeared, one can index the discreet distributions within each stimulus paradigm. In this past study, n and p was estimated for stimulation frequencies of 1Hz, 2Hz, and 3Hz. The findings showed that as the stimulation frequency increased, new sites are recruited (thus an increase in n) and the probability of release (p) increased for each site. It should be noted that in this past study the recordings were made over the varicosities with many synapses and AZs, whereas in this current study 4–9 synapses are monitored with relatively few AZs present.

The objective of this study was to serially reconstruct, at the ultrastructure level, the synapses and associated AZs in low output regions of the nerve terminal in which quantal recordings were obtained with varying stimulation frequencies to determine if quantal signatures could be assigned to the few synapses present. We attempted to compare the number of AZs and clusters of potential quantal signatures with the aim to help in defining vesicle fusion statistics in probability (p) of release and number of quantal release sites (n) to synaptic structural complexity.

METHODS

General

All experiments were performed using the first and second walking legs of crayfish, *Procambarus clarkii*, measuring 6–10 cm in body length (Atchafalaya Biological Supply, Raceland, LA). Animals were housed individually in an aquatic facility and fed dried fish food. Dissected preparations were maintained in crayfish saline, a modified Van Harreveld's solution (in mM: 205 NaCl; 5.3 KCl; 13.5 CaCl₂·2H₂O; 2.45 MgCl₂·6H₂O; 5 HEPES adjusted to pH 7.4). Crayfish were induced to autotomize the first or second walking leg by forcefully pinching at the merus segment. Details of the dissection and equipment used are shown in video format (Cooper and Cooper, 2009).

Identification and marking of stem regions

To identify the low output stem area of the motor neuron, the vital dye 4-Di-2-Asp (Molecular Probes) was used. This dye highlights the neuron, which allows the focal macropatch, to be placed at a specific

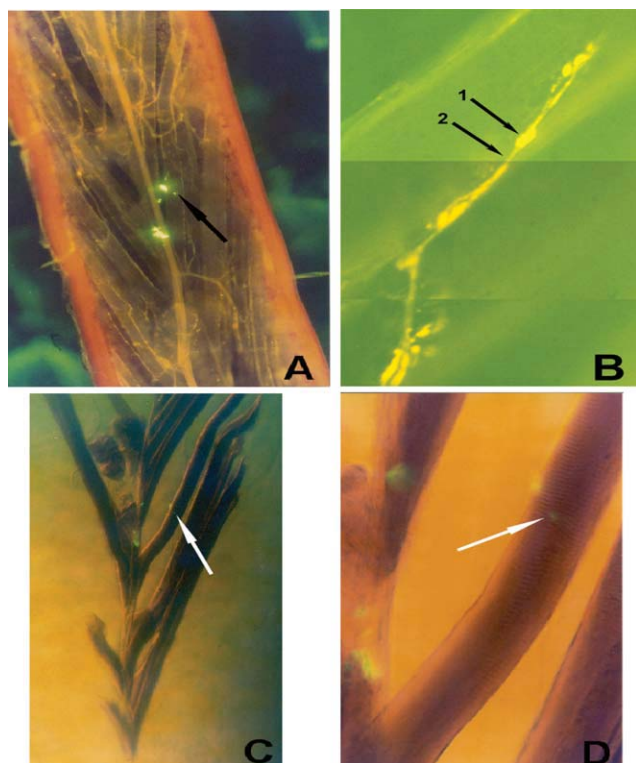


Fig. 1. Stem preparation. (A) Opener muscle stained with 4-di-2-Asp. Polystyrene beads present from rim of focal electrode and area specifically recorded (arrow). (B) High magnification of muscle fiber stained with 4-di-2-Asp showing nerve terminal innervation with varicosities (1) and stem regions between varicosities (2). (C) Low magnification of dissected, fixed and trimmed opener muscle showing the region recorded from with a focal electrode (white arrow). (D) Higher magnification of C, region recorded (white arrow).

site – the stem (Cooper et al., 1995b; Cooper and Cooper, 2009). Using this approach also allows the specific site to be labeled for thin sectioning (~100–120 nm) by using fluorescent and electron dense beads either by preloading them around the lumen of the patch electrode or after a recording is made to label the site. If the electrode is precoated before recording then when the patch electrode is removed, a ring of beads is left behind, marking the site (Fig. 1A) This method was previously used to rebuild complex synapses at high and low output varicosities to identify the number of AZs between them (Cooper et al., 1995b, 1996b). In Figure 2 (between the arrows), a long stem region is shown that appears to be devoid of large varicosities. Such long stem regions are not common but they do provide an opportunity to investigate regions with fewer synapses.

Physiology

To elicit an evoked response, the excitatory axon was selectively stimulated by placing a branch of the leg nerve (from the merus segment) into a suction electrode connected to a Grass stimulator (see Cooper and Cooper,

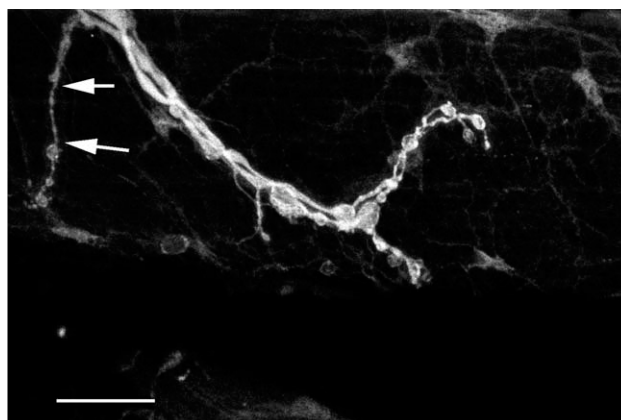


Fig. 2. A stem region shown in a preparation staining with 4-di-2-Asp. This is shown in black and white for enhanced contrast. Here the stem region is quite pronounced located between the two arrows. Note slight swellings but very reduced as compared to the larger varicosities. Scale bar = 20 μm .

2009 for visual details; Dudel and Kuffler, 1961). The possibility that presynaptic and postsynaptic inhibition altered the responses during these experiments, due to spontaneous fusion of vesicles in the inhibitor neuron, is extremely low given that evoked release in the excitatory terminals is at a set frequency and that the release was extremely low in probability. Thus, the possibility of two low probability events, with one being random in nature, occurring simultaneously is very low.

Field excitatory postsynaptic potentials

Synaptic field potentials were measured with focal macropatch electrodes to assess presynaptic vesicular events. It was demonstrated in an earlier report that 4-di-2-ASP had no effect on transmission with the concentration (5 μM) used in this study (Cooper et al., 1995a). The synaptic potentials were obtained using the loose patch technique by lightly placing a 10–20 μm fire-polished glass electrode directly over a spatially isolated varicosity along the nerve terminal. The field excitatory postsynaptic potentials (fEPSPs) and field miniature excitatory postsynaptic potentials (fmEPSPs) can readily be recorded (Cooper et al., 1995b, 1996a; del Castillo and Katz, 1954a). One might assume the conditions for quanta would be similar for a fusion site in respect to focal electrode placement when measuring the field potential. However, varying distance from the source and recording along with the distortion by subsynaptic reticulum can have an effect on the shape of the responses. Thus, each postsynaptic array response to vesicle fusion could have a unique profile. We assume the field potential parameters will stay constant throughout the experiment, for a given fusion site, and thus we can monitor the frequency of occurrences and characteristics in their shape as well as if new shapes appear.

Electrical signals were recorded on-line to a Power Mac 9500 or to a Dell Latitude D600 computer via a

MacLab/4s or a PowerLab/4s interface, respectively. In addition, to direct quantal counts the quantal characteristics were measured as described later.

Quantal analysis

Quantal analysis was carried out with the assistance of a statistical program written in R language (Lancaster et al., 2007). This program has the ability to use single events and account for DC shift to create a baseline using the tails of traces that have a low occurrence of events, and to automatically measure different parameters of quantal events: Area under the event, rise time, peak amplitude, tau decay, and latency. The traces are inverted in this report for ease in analysis. The amplitudes of the quantal responses are arbitrary as electrode seal resistance among preparations is variable. In addition, the traces are relatively scaled for comparisons within a preparation.

We collectively refer to the variables area under the curve (AUC), rise time, peak amplitude, tau, and latency as functionals (aspects of a function, we avoid the use of “parameter” as these functionals do not fully define the quantal responses). Our goals are to determine (1) any change in the mean quantal content across different stimulation frequencies, and (2) any change in the functionals across different stimulation frequencies.

Transmission electron microscopy

All preparations were fixed in a 2.5% glutaraldehyde, 0.5% formaldehyde buffered solution (0.1 M sodium cacodylate, 0.022% wt CaCl_2 , 4% wt sucrose, and adjusted to pH of 7.4) for 1 h with two changes and post fixed with a 2% osmium tetroxide buffered solution and embedded in Eponate 812. The samples were serially thin sectioned on a Reichert ultracut microtome and post stained with uranyl acetate and lead citrate. Sections were then viewed on a FEI: Philips Tecnai, Bio Twin 12 model transmission electron microscope at 80 or 100 kV.

Preparation of formvar coated grids

To ensure that grid bars from commonly used EM grids would not interfere with the site of interest, slotted nickel grids (1 mm \times 2 mm), were coated with 1% formvar (Electron Microscopy Sciences, EMS). These grids were used to capture sections prior to coating. Formvar dissolved in di-ethylene chloride was used to coat noncharged, precleaned slides using a film-casting device (EMS). Once coated, the slide was quickly dried using a heat lamp. A razor blade was then used to scrape the edges of the coated slide. Warm/moist air was then blown on the edge of the slide to loosen the formvar from the slide. The slide was then dipped at $\sim 35^\circ$ angle into distilled water,

which allowed the formvar to separate from the slide leaving it floating on the water's surface.

The detached formvar was then collected using a domino rack (EMS), a plastic coated platform with holes that are slightly larger than an EM grid (3 mm in diameter). This allows the holes to be covered by the formvar. The domino racks were then slowly dried at room temperature in clean glass dishes over night.

The resin block with the embedded tissue was then trimmed to a block face of $\sim 0.25 \text{ mm}^2$, cut with a diamtome 3-mm diamond knife at a 6° cutting angle. Serial sections were then collected in three section increments. These sections were then collected from the diamond knife boat with a slotted grid (held in the slot by water cohesion) held by forceps and gently placed on the domino rack coated with formvar. Once a domino was full, it was placed back into the glass dish and placed in an oven ($\sim 37^\circ$) to evaporate any remaining water and to promote the nickel grid to adhere to the formvar.

Once dry, grids (with sections) were removed from the domino rack using a 2.5-mm acu-punch biopsy tool (Acuderm). The grids were then placed in a Hiroki staining flat and stained in a Hiroki staining dish (EMS) using the staining procedure described in the transmission electron microscopy methods.

Measurements for synapses and AZ distribution

Each transmission electron micrograph that revealed a synapse was cataloged. In some cases, complete serial sections of synapses were obtained. The presynaptic terminals were classified as excitatory by the shape of the vesicles as well as if presynaptic inhibition was present. Inhibitory terminals reveal oblique shaped vesicles (Tse et al., 1991) and were not further used for quantification. The appearance of dense bodies associated with synapses within the presynaptic terminal was used to define an AZ. Within the crayfish NMJ, AZs are places where vesicles cluster in association to fusion with the presynaptic membrane (Cooper et al., 1996b). These dense bodies are thought to serve as cytoskeleton attachment points to deliver tethered synaptic vesicles possible from reserve pools. The presence of presynaptic inhibition was evident in two of the three reconstructed stems. Presynaptic inhibition is a phenomenon in which the inhibitory motor neuron has synapses on excitatory neurons; thus, a neuron with a synapse onto another neuron, with an AZ present, would indicate it as the inhibitor (Fig. 3), since no presynaptic excitation from the excitor to the inhibitor has ever been established. Figure 4 illustrates an active zone on one synapse and a synapse with docked vesicles but no active zone within this particular section.

Synapses at the crayfish NMJ do not have a grid of AZ on the synapses but show synaptic variation such that some synapses may only possess a single AZ

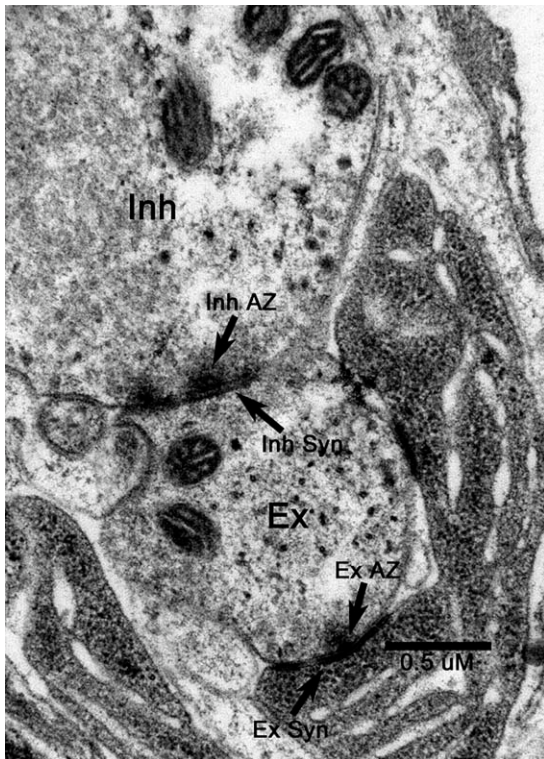


Fig. 3. Identification of the excitor stem for 3D reconstruction (section from stem 2). Electron micrograph of the excitor stem (Ex) innervated by the inhibitor neuron (Inh) showing presynaptic inhibition. The inhibitor synapse (Inh Syn) reveals an AZ (inh AZ) as well as the exciter synapse (Ex Syn and Ex AZ). Scale bar = 0.5 μm .

while others might have multiple AZs at varying distances from one another (Cooper et al., 1996a,b). This is an important distinction if one is counting vesicle populations and locations as vesicles cluster around AZ's. In the crayfish opener preparation, the dense bodies of the excitatory terminals are viewed as hemispheres of about 60 nm in diameter sitting with the cross section of a hemisphere facing the synapse (Atwood and Cooper, 1994). This is documented by the occasional on face view in parallel sectioning of synapses (Cooper et al., 1996b). Thus, in 100–120 nm cross-section thickness a dense body can be contained within a single section. If the dense body is seen within two sections then sections either side of the section with the dense body were also used for analysis. Care for stereological errors in measuring objects in TEM from 2D images of 3D tissue was implemented as previously described (Atwood and Cooper, 1996; Feuerverger et al., 2000; Johnstone et al., 2008; Kim et al., 2000).

RESULTS

Quantal measures and characteristics

Five opener stem preparations were recorded for quantal analysis, three of which were rebuilt through



Fig. 4. An electron micrograph of a section of terminal which depicts two synapses. On one synapse an enhanced dense structure is clearly seen with vesicles clustered around it. This is referred to as an active zone. The synapse at the top of the figure shows docked vesicles but no active zone. Scale bar = 0.5 μm .

electron microscopy. The macropatch technique was used to record quantal events from the stem region between two varicosities of the excitor neuron. To study quantal characteristics among single evoked events, a low output region of innervation and a relative low frequency of stimulation paradigm were used. Each stem was recorded for ~ 2000 evoked stimulations at 1, 2, and 3 Hz, which gave rise to different synaptic responses. Figure 5 shows what types of responses that are seen during a typical recording period. Each trace has two characteristics in common, one an artifact (arrow 1), due to the stimulus traveling through the saline bath and two, a spike (arrow 2) which represents the field response of the presynaptic action potential (i.e., spike) recorded under the patch electrode traveling along the nerve terminal. After the spike, the majority of trial runs show a failure (Fig. 5A), but some traces show single (Fig. 5B) or multiple events (Fig. 5C). Since the interest is in characteristic shapes of single events for this study, these multiple events were not analyzed, but are included in the mean quantal content. Also spontaneous events known as minis occur (Fig. 5D). These are events that occur randomly and are not due to the evoked stimuli. These minis were also not analyzed and not included in the mean quantal content. The single evoked events were analyzed using the R quantal analysis program (see Lancaster et al. 2007 in

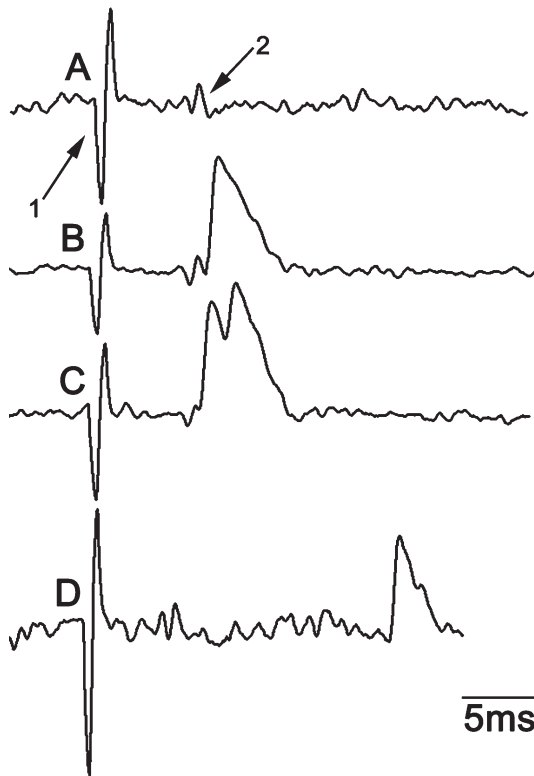


Fig. 5. Quantal analysis: (A) Trace representing a failure, recorded as 0, not analyzed. 1: Artifact. 2: Spike. (B) Trace representing a single evoked event (occurring directly after the spike), recorded as a single event. (C) Trace representing a multiple event (in this case a doublet), recorded as two events. (D) Trace representing a spontaneous event, but a failure in evoking an event, not analyzed. These traces are from different sites and shown here to highlight the varied types of responses.

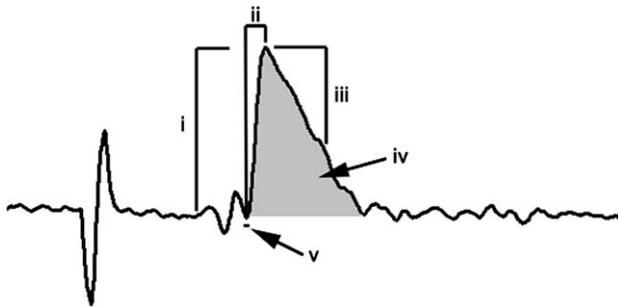


Fig. 6. Parameters that are measured from single quantal events. i: Peak amplitude. ii: Time to reach peak amplitude. iii: Tau decay time. iv: (gray) Area of the event. v: Latency from the spike.

methods). This allowed relatively quick computation of mean quantal content, area of each event, as well as peak amplitude, latency, tau decay, and time to peak amplitude (Fig. 6). Table I shows the mean quantal content of each stem at 1 Hz to 3 Hz broken down into single events (indicated by "1"), multiple events (marked as numbers, each representing the number of event during that run), total number of traces analyzed (N) and mean quantal content (m).

Synapse

TABLE I. Quantal analysis of the five stems that were recorded from

	1 Hz	2 Hz	3 Hz
Stem 1			
0	1701	1904	1847
1	163	92	124
2	3	2	4
N	1867	1998	1998
m	0.091	0.048	0.066
Stem 2			
0	1841	1829	1924
1	150	168	72
2	3	1	1
3	2	0	1
N	1996	1998	1998
m	0.081	0.085	0.039
Stem 3			
0	1865	1946	1936
1	125	52	54
2	4	0	0
3	1	0	0
8	1	0	0
N	1996	1998	1990
m	0.072	0.026	0.027
Stem 4			
0	1823	1808	1860
1	170	187	129
2	5	3	8
3	0	0	1
N	1998	1998	1998
m	0.090	0.097	0.074
Stem 5			
0	1866	1859	1859
1	85	117	127
2	14	18	3
3	2	3	5
4	0	1	3
5	1	0	0
N	1968	1998	1997
m	0.063	0.083	0.080

Each stem was analyzed using the automated firing program to analyze single events (1's). The raw data was also visually inspected to find all multiple firings as well (doublets, triplets, etc.) so mean quantal content could be assessed. The first column states the number of discrete events (0, failures; 1, single events; 2 double events; etc.) that occurred per stimulus trial. The remaining columns state the observed number of occurrences during each frequency (1-3Hz), 1998 trial for each frequency. Row n: Because some traces are problematic to analyze, for a multitude of reasons, they must be thrown out (not counted), N represents the number of useable traces for each frequency. The mean quantal content (m) for each condition is shown for each of the total number of trials.

Analysis of mean quantal content and the individual functionals (area, peak amplitude, etc. . .) was conducted using stems as random effects (e.g., the stems were assumed to be drawn from a greater population and thus the variation across stems is accounted for in the analysis) and the stimulation frequency (hertz) as a fixed effect. In the results we show there is substantial variation across stems, but that the effect of stimulation frequency is significant even after accounting for that variation.

The mean quantal content was analyzed using a generalized linear model (here Poisson regression) version of a repeated measures ANOVA. The number of quanta in each condition (see Table I) was analyzed using stem as a random effect and hertz as a fixed effect. Note in a Poisson regression the log of the mean number of quanta per stimulation is the parameter of interest. This analysis indicates the mean quantal content is reduced as the stimulation frequency is increased

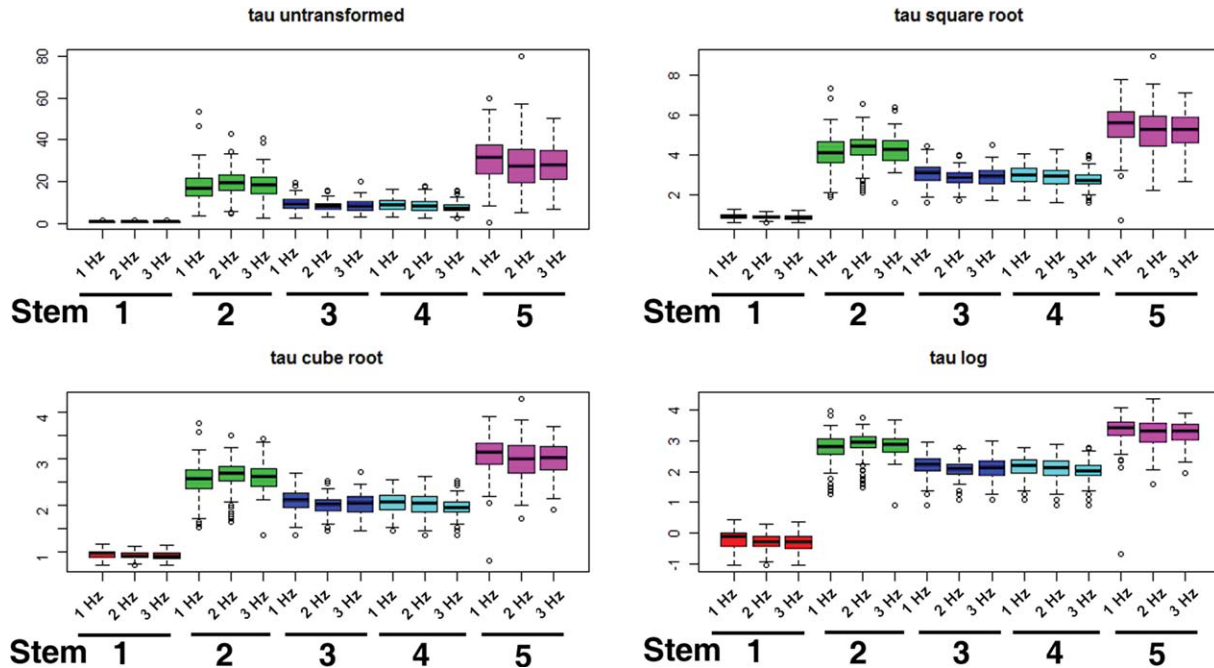


Fig. 7. This figure illustrates the raw data for tau (upper left panel) and three possible transformations (square root, cube root, and log). The stems are separated by colors, with the three boxplots in each color indicates the 1, 2, and 3 Hz stimulation frequencies. Clearly there are problems with changing spread in the untransformed data. The log transformation was chosen to most stabilize the variation. The remaining functionals (AUC, rise time, latency, and peak amplitude) showed qualitatively similar patterns.

(overall $P < 0.0001$, estimated contrast 2–1 Hz is -0.157 with $P = 0.003$ and estimated contrast 3–1 Hz is -0.325 with $P < 0.0001$). These parameters refer to the log of the mean quantal content and thus are on a “percentage” scale, the (-0.157) indicates mean quantal content at 2 Hz is only $\exp(-0.157) = 85.5\%$ of mean quantal content at 1 Hz. At 3 Hz, mean quantal content is only $\exp(-0.325) = 72.2\%$ of the mean quantal content at 1 Hz.

Each functional was transformed to the log scale before conducting the repeated measures ANOVA because of obvious issues with changing variances. In Figure 7, we see various transformations of tau (the other functionals are qualitatively similar). In the untransformed data, we can see the clear differences among the stems, and that the variation varies greatly from stem to stem. Figure 7 also illustrates some possible transformations. The log transformation was chosen because it appears to stabilize the variance the most.

Repeated measures ANOVA were then fit separately using the log of each functional as a response variable, the stem as a random effect, and the stimulation frequency as a fixed effect (fitted as a factor variable). Table II shows the results of this analysis. For each functional we find similar results: specifically (1) there is considerable variation across stems, accounted for in the repeated measure ANOVA and (2) the functionals,

TABLE II. Results of the repeated measures ANOVA for each of the five functional

Functional	Hertz contrasts	P -value for Hertz	Standard deviation across stems
log(AUC)	-0.072 (2–1 Hz)	0.001	0.660
	-0.150 (3–1 Hz)		
log(latency)	-0.010 (2–1 Hz)	0.006	1.076
	-0.162 (3–2 Hz)		
log(peak)	-0.055 (2–1 Hz)	0.002	1.255
	-0.112 (3–1 Hz)		
log(rise)	-0.054 (2–1 Hz)	0.019	0.429
	-0.067 (2–1 Hz)		
log(tau)	-0.025 (2–1 Hz)	0.018	1.368
	-0.067 (3–1 Hz)		

For each functional we can see the significant variation across stems (column 4), the statistical significance of the stimulation frequency (column 3), and the contrasts between the different stimulation frequencies (column 2). For reference, a difference of -0.10 on the log scale indicates values that are $\exp(-0.10) = 90.5\%$ as large on the actual scale of the data.

in general, decrease as the stimulation frequency is increased which suggest synaptic depression over time.

The second column in Table II shows the contrasts between 2 and 1 Hz and between 3 and 2 Hz. Thus, for example, looking at the AUC data we find 2 Hz averages 0.072 lower than 1 Hz while 3 Hz averages 0.150 lower than 1 Hz. A difference of 0.15 on the log scale indicates the 3 Hz data is $\exp(-0.15) = 86\%$ as large as the 1 Hz data after accounting for differences in stems.

Solely for visualization purposes, Figure 8 shows the “stem-adjusted” values for each of the five func-

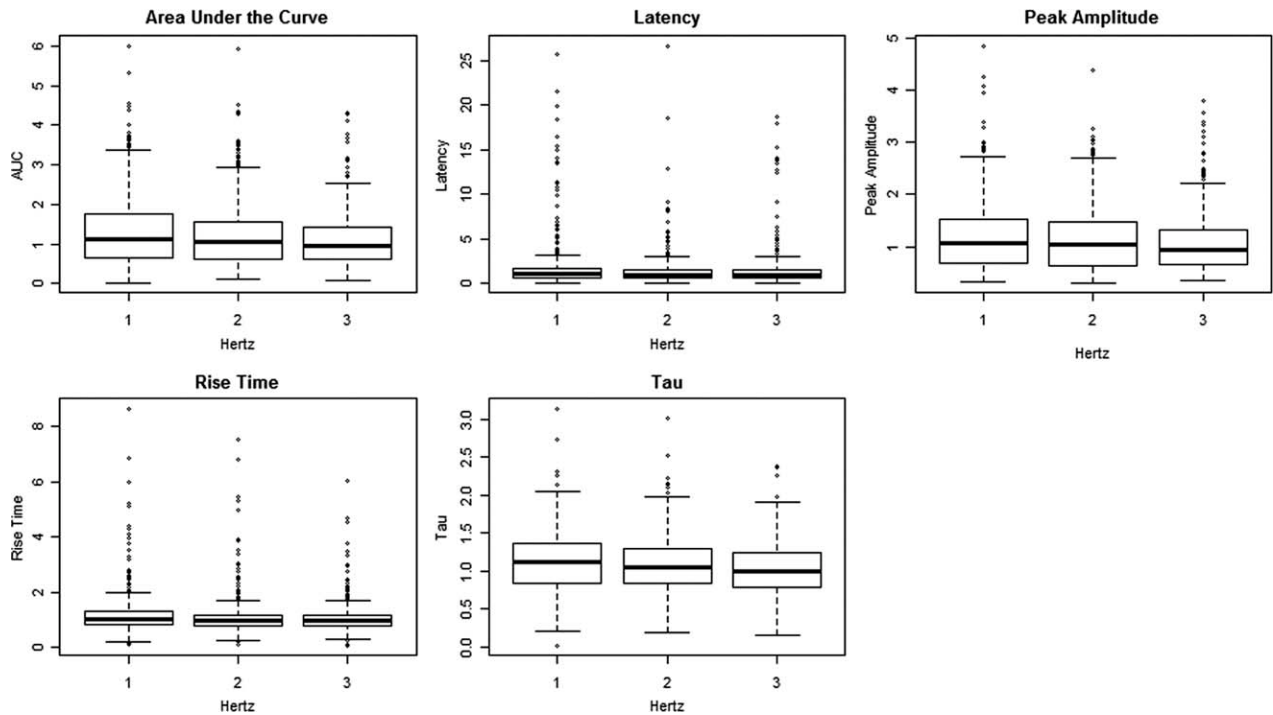


Fig. 8. Illustration of the effect of stimulation frequency on area under the curve, latency, peak amplitude, rise time, and tau after adjusting for the effect of stem. This plot was constructed by (1) transforming to the log scale, (2) from each log value subtracting the mean log value for the corresponding stem, and (3) plotting the results on the original (nonlogged) scale. This plot is not appropriate for viewing the statistical analysis, which takes place on the log scale and fully incorporates the variation across the stems as a random effect. However, the purpose here is to illustrate the general decreasing trend in each functional as the stimulation frequency is increased.

tionals. These plots were constructed by (1) taking the log value for each functional as described earlier, (2) subtracting the mean log value for each stem from each log value, which standardizes the results across stems, and then (3) plotting the adjusted values on the original (nonlogged) scale. Note these are not the values used in the analysis, as the log values are more appropriate for statistical treatment as described above. However, this plot is useful for visualizing the effect of stimulating frequency with the effect of stem removed, in particular the moderate percentage reduction in each of the functionals as the stimulation frequency is increased.

Anatomical analysis

The next part of this study was to rebuild the recorded region in order to reveal the actual number of synapses, AZ's as well as measure synaptic area and distance between AZs. Figure 9 shows a 3D representation of stem-1 rebuilt from electron micrographs. Each color represents a different synapse and each synapse is represented two-dimensionally to the sides of the stem. The lines represent the synaptic midlines from the sections while the ovals represent relative AZ location, while dashed lines represent sections that were unable to be salvaged.

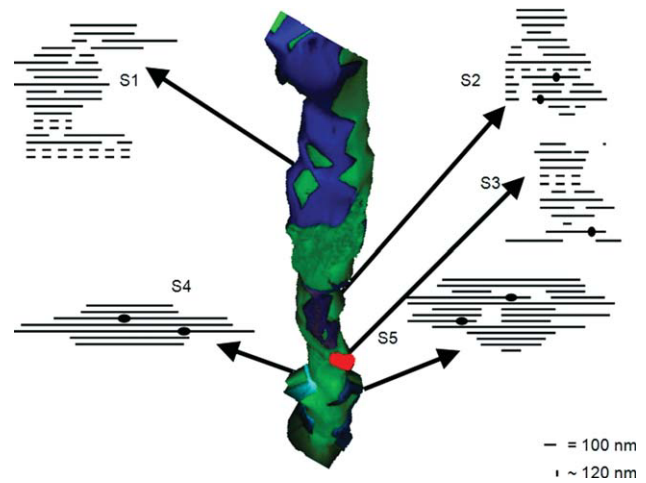


Fig. 9. Reconstruction of STEM 1 from electron micrographs. Five synapses were found on STEM 1 (S1–S5), each represented by a different color as well as two-dimensional representation (line diagrams). Each line represents the synaptic midline for that section. Active zone location is indicated by an oval for each synapse.

When considering the synaptic area, measurement of error was considered since stereological issues are relevant. A 3D object represented in 2D planes presents special requirements to deal with potential error in making measurements. When dealing with the synaptic ends via TEM, the last section portrays a

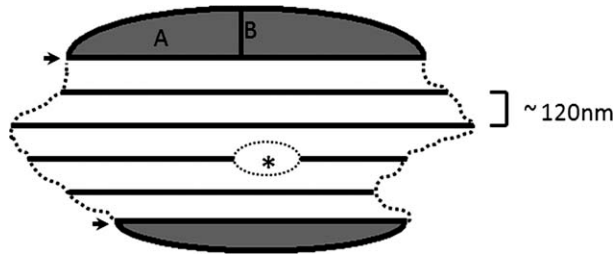


Fig. 10. Diagram depicting a synapse without AZ's to highlight parameters used to measure synaptic area. Arrowheads: representing the first and last sections of the synapse. Area in gray: Error measurement for the edge of the synapse using the ellipse formula divided by 2: $((\pi \times A \times B)/2)$. Dotted line: Hypothetical edges of synapse. Asterisk: Hypothetical perforation contained within one section. Bracket: measurement between the edges of two adjacent sections, ~ 120 nm.

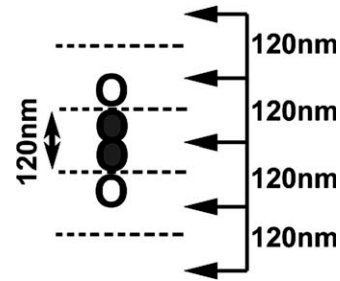


Fig. 11. Diagram depicting a synapse that is observed over 5 sections (arrows) with 2 AZ's (gray circles) showing the potential range the AZ may be located in a ~ 120 nm section (empty circles). The minimum distance is 0 nm, while the maximum distance is 120 nm (closest AZ edge). Dotted lines represent section midpoints where the center of the AZs is assumed to lie.

TABLE III. Measurements made from Stem reconstructions

Stem	No. of sections	% Capture	Syn	Syn area (μm^2)	Syn area (μm^2) w/Err	Diff	AZ	AZ Dis (μm)
1	75	83	1	14.67	14.76	0.09	0	
			2	8.21	8.4	0.19	1	
			3	6.55	6.84	0.29	1	0.578
			4	4.03	4.104	0.07	2	0.549
			5	11.36	11.49	0.13	1	4.104
2	72	78	1	3.48	3.64	0.16	1	
			2	0.019	0.0428	0.02	2	0.602
			3	0.918	0.983	0.06	1	
			4	4.53	4.64	0.11	2	1.281
							2	0.362
							3	0.632
			5	0.0263	0.0736	0.05	1	
			6	7.61	7.726	0.12	1	
			7	7.87	7.96	0.09	1	
8	2.34	2.379	0.04	1				
9	2.31	2.379	0.07	1				
3	106	70	1	5.22	5.88	0.66	0	
			2	8.68	9.19	0.51	1	
							2	0.399
							3	0.6
				3	0.73			
			3	0.752	0.8518	0.1		
			4	1.154	1.295	0.14		

Stem: indicates which stem is being measured. No. of Sections: total number of thin sections made to reconstruct stem region. %Capture: percent of sections that were able to be saved and analyzed. Syn: Number of synapses on each reconstructed stem. Syn Area: The area (μm^2) each of the synapses cover on the reconstructed stem. Syn Area w/ Err: The possible total area of the synapse, taking into account the error of the section thickness (μm^2) (Fig. 5). Diff: The difference in observed area and area accounting for error. AZ: The number of active zones per synapse, if present. AZ Dis: The observed distance between active zones on each synapse ($\pm 60\text{nm}$ error).

blunt end, while a synapse from sections obtained in parallel to the plane are known to be curved on their edges. The process of correcting the error measures are shown in Figure 10 and accounted for in Table III. In addition if a section was lost that occurred at the end of a synapse, the last section with a synapse present was treated as the edge of the synapse.

Not only was error of synaptic area calculated for but also AZ distance error. Because the section is

~ 100 – 120 nm in thickness, and an AZ is 60 nm in diameter, it is possible for an AZ to be located within any part of the section thickness, thus there is a degree of error to be accounted for with consideration for section thickness (Fig. 11). The maximum distance and minimum distance was calculated and included in the overall analysis of AZ distance (Table III).

Table III shows all the calculations of the rebuilt stems in which electrophysiological recordings were made. In Table III, the stem number is listed in the first column. Each stem was not completely rebuilt because some sections are lost during thin sectioning. The number of total sections accounted for are listed in the second column, while the third column gives the percentage of those sections that were actually accounted for and analyzed. Synapses are numbered for each stem and the synaptic area is reported with the error in the proceeding columns. The difference is calculated in the following column. Each stem had a range of synapses (4–9) and had a range of AZ's (0–14) in which the distance error between them was accounted for in the remaining columns. The largest synaptic area recorded was $2.379 \mu\text{m}^2$ (including error), while the smallest was recorded as $0.0428 \mu\text{m}^2$ (including error), these two extremes were also found within the same stems suggesting uniqueness in individual stems. The distance between AZ's on single synapses varied between stems. For stem 1, the minimum AZ distance was $0.6 \mu\text{m}^2$ and maximum was $0.73 \mu\text{m}^2$. For stem 2, the minimum distance was $0.549 \mu\text{m}^2$, and minimum was $4.104 \mu\text{m}^2$. Stem 3, minimum $0.399 \mu\text{m}^2$ to a maximum of $1.281 \mu\text{m}^2$.

DISCUSSION

In this study, it was attempted to correlate structure and function of nerve terminals and to increase the accuracy of quantal analysis, by utilizing a nerve terminal region that has low synaptic efficacy (i.e., the stem region). The stem region is located between varicosities and has been shown by this study and

others to have fewer synapses and fewer AZ than within varicosities. Florey and Cahill (1982) reconstructed the nerve terminals in the crayfish *Astacus leptodactylus*, and found the varicosities had about 10 synaptic sites and the stem regions had about ~2–3, while with the crayfish *Procambarus clarkii*, varicosities contained up to 50–60 synapses (Cooper et al., 1995b). In this study, it was determined that the stem regions contained four to nine synapses (in a length of 10 μm of the stem) and anywhere from 0 to 14 AZs (a synapse with no active zone is known as a blank synapse). This indicates species differences in nerve terminal innervations. The stem regions were specifically used in this study to intentionally reduce the number of release sites (n) to remove confounding variables such as large number of synapses, each of which could contain a multitude of AZs (Cooper et al., 1996a,b). Such synaptic complexity causes difficulty in delineating the number of release sites (n) and/or the probability (p) of each release sites from the quantal recordings. Classically, m was calculated by counting the number of observed events, all events being considered equal, over the number of stimulation trials. This study provides direct structural comparisons to physiological responses obtained from defined synaptic regions, while considering the different parameters of each singly evoke event, which enhances the understanding of synaptic physiology.

It had previously been reported the complexity in the AZ spacing on synapses could present varied calcium distribution and thus affect the probability of vesicle fusion (Cooper et al., 1996b). In varicosities, it was shown that as stimulation frequency increased the mean quantal content also increased. This suggested that new synaptic sites might be recruited as the stimulation frequency increased (Viele et al., 2003), but because of the large number of potential release sites, to make a prediction of which quantal signature came from which synapse was impractical. When analyzing data from the stem region we found that this region does not respond in the same manner as the varicosities in previous studies. The m generally decreased with an increase in stimulation frequency and in most cases the parameters measured for each quantal response (area, rise, peak, time to peak, and latency), had a slight decrease, over the stimulation frequencies (1–3 Hz). The preparations in which the quantal parameter correlations were made to structure is suggestive that the number of synapses is not related to quantal signatures. The possible variables that give rise to quantal variation may be too confounding to determine possible quantal signatures for a particular AZ or synapse even in this synaptically reduced preparation.

The stem region functions synaptically different from the varicosity in relation to m and correlation to stimulation frequency. Why this region responds dif-

ferently is not known. The first obvious difference between the varicosity and the stem region is size. Varicosities can be up to 5 μm in diameter, while the stem region ranges from 0.5 to 1.5 μm . Just this size difference may alter the way calcium is buffered and extruded as was shown for the thin phasic (high output) terminals as compared to tonic (low output) terminals on the extensor muscle of crayfish (Millar et al., 2005; Msghina et al., 1999).

An additional difference in the stem regions and the varicosities is that the larger volume in the varicosities are able to accommodate a pool of reserve vesicles where as in the stem regions there does not appear to be reserve pool that can be pulled from. This might account for differences in the rate of depression with frequency of stimulation between these regions. Separate pools of presynaptic vesicles are segregated based on their location and function. Various reports named the pools differently; therefore, no absolute definitions have been established. Nevertheless, the physiological and anatomical separation of two vesicle pools, reserve pool (RP) and readily releasable pool (RRP), are widely utilized as working models to address synaptic vesicle recycling. RRP is defined as a group of vesicles close to the synaptic active zones which will fuse and release neurotransmitter immediately responding to Ca^{2+} influx, while RP is a group of vesicles slightly further away from the synaptic face (about 100 nm in crayfish opener NMJ, the distance of two tightly touched vesicles). This pool is recruited under particular circumstances such as high-frequency stimulation or in the presence of neuromodulators, such as serotonin (Sparks and Cooper, 2004). All the vesicles are randomly distributed inside of the terminal without a clear separating line to distinguish RRP from RP. The differences between vesicles in a RP of the stems and varicosities are again similar to the anatomical differences between thin phasic and tonic terminals (Johnstone et al., 2008).

Because Ca^{2+} is buffered and removed in multiple ways within varicosities such as by ER, mitochondria, buffering proteins, and removal methods (i.e., PCMA and NCX) (Scheuss et al., 2006), the Ca^{2+} may be removed quickly as not to have as great of an effect on neighboring synapses and AZs. In the stem region, event variability does not seem to increase as drastically with low stimulation (1–3 Hz) as it does in the varicose region (Viele et al., 2003). If the abundance of these Ca^{2+} buffering/extruding systems are fewer in number in this region then calcium could increase rapidly with maintained stimulation (see review by Atwood et al., 1997). In such a small volume, such as in the stem region, it may be possible that Ca^{2+} affects each site equally, thus recruitment of new synapses or AZs would be masked, regardless of stimulation frequency. It was previously shown in the opener

motor neuron the amount of calcium in the terminal varicosity increases with stimulation frequency (Cooper et al., 1995a; Crider and Cooper, 2000). Sodium also increases with stimulation frequency (Winslow et al., 2002), which has been shown to have an effect, but not directly in LTF (Atwood and Tse, 1988). Thus, higher $[Ca^{2+}]_i$ and $[Na^+]_i$ during stimulation and potentially differential decay of the ion concentrations in the stem as compared to the increased volume of the varicosity are likely to be different.

An additional observation from the data recorded from the stem is that in most cases the mean quantal content decreased overall from 1 to 3 Hz (stems 1, 2, and 4). Because this is at low-frequency stimulation, it might be possible that the stem region is more susceptible to low frequency depression (LFD) than the varicose region (Takeda and Kennedy, 1965). This is a phenomenon, in which the neuron depresses in response to very low frequencies (0.0016–0.2 Hz), much lower than used in our study, but this possibility cannot be ruled out since this study was done at a region other than the varicosity and has not previously been investigated for LFD. The overall mechanism of LFD is unknown, but it is recognized to be a presynaptic phenomenon and phosphorylation-dependent, as shown through kinase inhibition (Silverman-Gavrila et al., 2005). If this is the case, then second messenger cascades must be considered to be involved. Considering that such activation of second-messengers could have a greater impact in the stem with a smaller reserve pool of vesicles as compared to the varicosity might be worth future consideration. In the micrograph shown, as well as others obtained from the stem region, the overall structure in the longitudinal core is occupied largely with microtubules and few synaptic vesicles. In varicosities there are many vesicles within the center (Cooper et al., 1995a, 1996a,b).

Synapses in the stem were observed without AZs, albeit there were missing sections, suggesting that silent synapses may be present at the stem region of the neuron. Silent synapses lack AZs are thought to be inactive at rest, but as shown in hippocampal neurons, they can be activated and AZ will appear if long-term synaptic plasticity is induced by repetitive stimulation through actin polymerization (Yao et al., 2006). Thus, they play a role in synaptic plasticity. Since it is possible they exist at the stem region, they may be a factor in the response recorded from the stem region, but because they were identified as silent even after the increase in the frequency (1–3 Hz), it is possible that they stayed silent and played no role in the stems recorded in the stimulation paradigm used in this study.

Another dynamic to the stem regions is that they are surrounded by much less subsynaptic reticulum.

This brings a postsynaptic component into play as well for the responsiveness in this region. With a varicosity, the entire surface is surrounded by subsynaptic reticulum with synapses occurring on any region. For instance, if a varicosity (treated as a sphere) is 5 μm in diameter the surface area associated with it is 78.5 μm^2 ($4\pi r^2$). While a stem (treated as a cylinder, with a length of 20 μm) the surface area is 31.8 μm^2 ($(2\pi r^2) + (2\pi r)h$). This is less than half the surface area of the varicosity, thus, more synaptic glutamate receptors (quisqualate-type) could be found surrounding the varicosity in the synaptic regions as compared to the stems synaptic regions. This provides another possible variable into the differing response with stimulation. Because of this difference in terminal size means the distribution of glutamate receptors, in synaptic regions, could easily be different at the stem region as compared to the varicosity. If one were to consider the postsynaptic receptor array being consistent in packing density, the exact location where a vesicle fuses with the synapse affects the amount of transmitter received by a specific area of the postsynaptic receptor array. Suppose the vesicle fuses on an edge of the presynaptic synaptic surface (Uteshev and Pennefather, 1997), the result would be a different size or shape of a recorded postsynaptic current (due to the entire quantal package not being deposited over the receptors) compared to a vesicle that released directly over the center of the array. In addition, one could also consider that a single quanta might saturate the postsynaptic array, thus, release from a synaptic edge would alter the quantal shape as would a subsequent central release. An edge release would not have a concentrated release over the receptors and would lose some glutamate due to spillover resulting in a smaller event. A subsequent vesicular release could result in a blunt peak, due to the glutamate receptors not being completely reset from the first release. The neighboring effect would likely be more substantial in the stem region than the varicosity with receptors farther apart.

The degree of subsynaptic reticulum could also alter the degree of amplification of the membrane potential due to differences in series resistance. Such a factor has not been addressed previously for regional differences along these types of varicose-stem terminals but has been investigated for a vertebrate NMJ in regards to the enfoldings in the plasma membrane of the muscle and degree of activation of voltage gated ion channels (Martin, 1994).

Synapses were found to have a range of AZs from 0 to 3 at the stem region. Thus, the stem region is still fairly complex and not as simplistic as we originally thought for studying structure and function of synapses in relation to correlating a quantal signature. Although, in the stems reconstructed, the AZs were

not in close enough proximity to imply that their calcium influx domains would impact the neighboring AZ according to previous computational models (Cooper et al., 1996b). This alludes to the possibility that when calcium enters the cell in the low frequency stimulation paradigm each AZ acts independent of the others. However, the buffering of calcium in the stem region needs to be considered and this has not been addressed specifically for this region in the previous computational assessment (Cooper et al., 1996b). This leads to the possibility that the calcium build up in the stem region would also mask the calcium cloud distribution between AZs and possibly whole synapses. Of course, it would have been ideal if a single synapse with a single AZ was obtained in the reconstructions as then one would know where the quantal responses had originated. In addition, mechanisms for variations, if present, in the quantal responses would have been able to be addressed with more substantive possibilities.

To more accurately estimate n and p from physiological and anatomical data, it is important to discuss what n actually refers to. Some investigators refer to n as an entire varicosity (Korn et al., 1981), while others count each synapse as n , yet some suggest each AZ (Faber, 1991; Redman, 1990). Since in this preparation each AZ can dock up to six to seven vesicles, as seen in freeze fractures as well as TEM sections obtained parallel to the synapse face (Cooper et al., 1995b, 1996a,b) one could consider each docking site as an n . Thus, a single AZ would have an n of 6–7 but each n in this case would have an equal probability of release so possibly a functional $n = 1$ could be assigned to an AZ. However, if a release occurs at one site its probability of a second release would be reduced for a period of time. This would alter the probability of neighboring sites within a given time period. If one considers each docking site as an n , then even a single AZ is complex to study in reference to p considering that the release at one site would be dependent on its own site's history and a neighboring site's history. Thus, the assumption that each site is independent would not be valid. This level of statistical investigation has not been tackled in the synaptic field properly. This is likely because of a lack of experimental measurements to address the issue.

Obviously there is a wide range in defining n . In this study, stems were recorded, which are located between varicosities and quantal events are able to be recorded thus, n does not necessarily mean individual varicosities, but could still account for synapses and AZs. In addition, because a quantal event is the result of a single vesicle fusing with the membrane (Fatt and Katz, 1952), it would be logical to say n is the area in which a vesicle fuses. Because a synapse can harbor a multitude of AZs, even in low output terminal areas, such as the stem region, one can-

not account for which AZ is "active" at a given time, thus we cannot define which synapse accounts for each n .

Because even the stem region of the tonic opener neuron is too complex, n cannot be determined yet from recorded characteristic parameters of quantal responses. Although, this study has offered insight into analysis of n and p as well as measures of quantal fluctuation in these simpler synaptic preparations, the hunt continues to find preparations with single synapses containing a single AZ to define quantal variation and structural/functional relationships. The quantal decay time at the larval *Drosophila* NMJ is shortened with increasing levels of external $[Ca^{2+}]$ (Pawlu et al., 2004). We did not observe a change in the decay rates of quantal responses with increasing stimulation frequency so this phenomenon might be unique only to *Drosophila* NMJs. Perhaps slowing down all the biochemical and physical properties, by a reducing the temperature, would amplify quantal differences that could be indexed. Such an approach remains to be tested with a focal recording over a defined varicosity or stem region in this preparation.

There are additional parameters that need to be accounted for in order to consider structure and function of nerve terminals and possible differences within the stem and varicose regions. Since many biochemical factors play a role in the overall function of synaptic transmission differential activation of cellular cascades needs to be considered over various stimulation paradigms. It is known that biochemical properties (i.e., second messenger cascades, calcium binding, phosphorylation events, etc) that affect m are likely acting through altering p at any given site (Dason et al., 2009; Dixon and Atwood, 1989; Sudhof, 2004; Xia and Storm, 2005; Yao et al., 2006).

ACKNOWLEDGMENTS

We thank Mr. Ronald Chase Southard at the University of Kentucky for his early contributions to quantal analysis on pilot projects leading up to this study.

REFERENCES

- Atwood HL, Cooper RL. 1996. Assessing ultrastructure of crustacean and insect neuromuscular junctions. *J Neurosci Methods* 69:51–58.
- Atwood HL, Cooper RL, Wojtowicz JM. 1994. Nonuniformity and plasticity of quantal release at crustacean motor nerve terminals. *Adv Second Messenger Phosphoprotein Res* 29:363–382.
- Atwood HL, Karunanithi S, Charlton MP. 1997. Strength of synaptic transmission at neuromuscular junctions of crustaceans and insects in relation to calcium entry. *Invert Neurosci* 3:81–87.
- Atwood HL, Tse FW. 1988. Changes in binomial parameters of quantal release at crustacean motor axon terminals during presynaptic inhibition. *J Physiol* 402:177–193.
- Augustine MP, Charlton MP, Smith SJ. 1985. Calcium entry into voltage-clamped presynaptic terminals of squid. *J Physiol* 367:143–162.

- Cooper RL, Marin L, Atwood HL. 1995a. Synaptic differentiation of a single motor neuron: Conjoint definition of transmitter release, presynaptic calcium signals, and ultrastructure. *J Neurosci* 15:4209–4222.
- Cooper RL, Stewart BA, Wojtcowicz JM, Wang S, Atwood HL. 1995b. Quantal measurement and analysis methods compared for crayfish and *Drosophila* neuromuscular junctions, and rat hippocampus. *J Neurosci Methods* 61:67–78.
- Cooper RL, Harrington CC, Marin L, Atwood HL. 1996a. Quantal release at visualized terminals of a crayfish motor axon: Intraterminal and regional differences. *J Comp Neurol* 375:583–600.
- Cooper RL, Winslow JL, Govind CK, Atwood HL. 1996b. Synaptic structural complexity as a factor enhancing probability of calcium-mediated transmitter release. *J Neurophysiol* 75:2451–2466.
- Cooper AS, Cooper RL. 2009. Historical view and physiological demonstration of synaptic transmission at the crayfish opener muscle. *J Visualized Exp (JoVE)* 33.http://www.jove.com/index/details.stp?id=1595; doi: 10.3791/1595.
- Couteaux RM, Pecot-Dechavassine M. 1970. Synaptic vesicles and pouches at the level of “active zones” of the neuromuscular junction. *C R Acad Sci Hebd Seances Acad Sci D* 271:2346–2349.
- Couteaux R, Pecot-Dechavassine M. 1974. Specialized areas of presynaptic membranes. *C R Acad Sci Hebd Seances Acad Sci D* 278:291–293.
- Crider ME, Cooper RL. 2000. Differential facilitation of high- and low-output nerve terminals from a single motoneuron. *J Appl Physiol* 88:987–996.
- Dason JS, Romero-Pozuelo J, Marin L, Iyengar BG, Klose MK, Ferrús A, Atwood HL. 2009. Frequentin/NCS-1 and the Ca²⁺-channel α 1-subunit co-regulate synaptic transmission and nerve-terminal growth. *J Cell Sci* 122 (Pt 22):4109–4121.
- Del Castillo J, Katz B. 1954a. Quantal components of the end-plate potential. *J Physiol* 124:560–573.
- Del Castillo J, Katz B. 1954b. Action, and spontaneous release, of acetylcholine at an inexcitable nerve-muscle junction. *J Physiol* 126:27.
- Dudel J. 1981. The effect of reduced calcium on quantal unit current and release at the crayfish neuromuscular junction. *Pflugers* 391:35–40.
- Dudel J, Kuffler SW. 1961. The quantal nature of transmission and spontaneous miniature potentials at the crayfish neuromuscular junction. *J Physiol* 155:514–529.
- Dixon D, Atwood HL. 1989. Phosphatidylinositol system's role in serotonin-induced facilitation at the crayfish neuromuscular junction. *J Neurophysiol* 62:239–246.
- Faber DS, Korn H. 1991. Applicability of the coefficient of variation method for analyzing synaptic plasticity. *Biophys J* 60:1288–1294.
- Fatt P, Katz B. 1952. Spontaneous subthreshold activity at motor nerve endings. *J Physiol* 117:109–128.
- Feuerverger A, Menzinger M, Atwood HL, Cooper RL. 2000. Statistical methods for assessing the dimensions of synaptic vesicles in nerve terminals. *J Neurosci Methods* 103:181–190.
- Florey E, Cahill MA. 1982. The innervation pattern of crustacean skeletal muscle. Morphometry and ultrastructure of terminals and synapses. *Cell Tissue Res* 224:527–541.
- Govind CK, Pearce J, Wojtcowicz JM, Atwood HL. 1994. “Strong” and “weak” synaptic differentiation in the crayfish opener muscle: structural correlates. *Synapse* 16:45–58.
- Hessler NA, Shirke AM, Malinow R. 1993. The probability of transmitter release at a mammalian central synapse. *Nature* 366:569–572.
- Heuser JE, Reese TS, Landis DM. 1974. Functional changes in frog neuromuscular junctions studied with freeze-fracture. *J Neurocytol* 3:109–131.
- Jahromi SS, Atwood HL. 1974. Three-dimensional ultrastructure of the crayfish neuromuscular apparatus. *J Cell Biol* 63(2 Pt 1):599–613.
- Johnstone AFM, Kellie S, Cooper RL. 2008. Presynaptic depression in phasic motor nerve terminals and influence of 5-HT on docked vesicles. *The Open Neurosci J* 2:16–23.
- Katz B, Miledi R. 1967. Ionic requirements of synaptic transmitter release. *Nature* 215:651.
- Katz B, Miledi R. 1968. The role of calcium in neuromuscular facilitation. *J Physiol* 195:481–492.
- Kim S, Atwood HL, Cooper RL. 2000. Assessing accurate sizes of synaptic vesicles in nerve terminals. *Brain Res* 877:209–217.
- Korn H, Triller A, Mallet A, Faber DS. 1981. Fluctuating responses at a central synapse: n of binomial fit predicts number of stained presynaptic boutons. *Science* 213:898–901.
- Kriebel ME, Keller B, Fox GQ, Brown O. 2000. The secretory pore array hypothesis of transmitter release. *Cell Biol Int* 24:839–848.
- Lancaster M, Viele K, Johnstone AFM, Cooper RL. 2007. Automated classification of evoked quantal events. *J Neurosci Methods* 159:325–336.
- Llinas R, Steinberg IZ, Walton K. 1981. Presynaptic calcium currents in squid giant synapse. *Biophys J* 33:289–321.
- Martin AR. 1994. Amplification of neuromuscular transmission by postjunctional folds. *Proc R Soc Lond B* 258:321–326.
- Millar AG, Zucker RS, Ellis-Davies GC, Charlton MP, Atwood HL. 2005. Calcium sensitivity of neurotransmitter release differs at phasic and tonic synapses. *J Neurosci* 25:3113–3125.
- Msghina M, Govind CK, Atwood HL. 1999. Synaptic structure and transmitter release in crustacean phasic and tonic motor neurons. *J Neurosci* 18:1374–1382.
- Pawlu C, DiAntonio A, Heckmann M. 2004. Postfusional control of quantal current shape. *Neuron* 42:607–618.
- Rao-Mirotnik R, Harkins AB, Buchsbaum G, Sterling P. 1995. Mammalian rod terminal: Architecture of a binary synapse. *Neuron* 14:561–569.
- Redman S. 1990. Quantal analysis of synaptic potentials in neurons of the central nervous system. *Physiol Rev* 70:165–198.
- Rheuben MB. 1985. Quantitative comparison of the structural features of slow and fast neuromuscular junctions in *Manduca*. *J Neurosci* 5:1704–1716.
- Rosenmund C, Clements JD, Westbrook GL. 1993. Nonuniform probability of glutamate release at a hippocampal synapse. *Science* 262:754–757.
- Scheuss V, Yasuda R, Sobczyk A, Svoboda K. 2006. Nonlinear [Ca²⁺] signaling in dendrites and spines caused by activity-dependent depression of Ca²⁺ extrusion. *J Neurosci* 26:8183–8194.
- Silverman-Gavrila LB, Orth PM, Charlton MP. 2005. Phosphorylation-dependent low-frequency depression at phasic synapses of a crayfish motoneuron. *J Neurosci* 25:3168–3180.
- Sparks G, Cooper RL. 2004. 5-HT offsets homeostasis of synaptic transmission during short-term facilitation. *J Applied Physiol* 96:1681–1690.
- Sudhof TC. 1995. The synaptic vesicle cycle: A cascade of protein-protein interactions. *Nature* 375:645–653.
- Sudhof TC. 2004. The synaptic vesicle cycle. *Annu Rev Neurosci* 27:509–547.
- Sugimori M, Lang EJ, Silver RB, Llinas R. 1994. High-resolution measurement of the time course of calcium-concentration microdomains at squid presynaptic terminals. *Biol Bull* 187:300–303.
- Takeda K, Kennedy D. 1965. The mechanism of discharge pattern formation in crayfish interneurons. *J Gen Physiol* 48:435–453.
- Uteshev VV, Pennefather PS. 1997. Analytical description of the activation of multi-state receptors by continuous neurotransmitter signals at brain synapses. *Biophys J* 72:1127–1134.
- Viele K, Stromberg AJ, Cooper RL. 2003. Estimating the number of release sites and probability of firing within the nerve terminal by statistical analysis of synaptic charge. *Synapse* 47:15–25.
- Vremsen G, Cardozo JN, Muller L, Van der Want J. 1980. The presynaptic grid: a new approach. *Brain Res* 184:23–40.
- Walrond JP, Reese TS. 1985. Structure of axon terminals and active zones at synapses on lizard twitch and tonic muscle fibers. *J Neurosci* 5:1118–1131.
- Winslow JL, Cooper RL, Atwood HL. 2002. Intracellular ionic concentration by calibration from fluorescence indicator emission spectra, its relationship to the Kd, Fmin, Fmax formula, and use Na-Green for presynaptic sodium. *J Neurosci Meth* 118:163–175.
- Xia Z, Storm DR. 2005. The role of calmodulin as a signal integrator for synaptic plasticity. *Nat Rev Neurosci* 6:267–276.
- Yao J, Qi J, Chen G. 2006. Actin-dependent activation of presynaptic silent synapses contributes to long-term synaptic plasticity in developing hippocampal neurons. *J Neurosci* 26:8137–8147.
- Zucker RS, Delaney KR, Mulkey R, Tank DW. 1991. Presynaptic calcium in transmitter release and posttetanic potentiation. *Ann N Y Acad Sci* 635:191–207.